Crossed-Wire Laser Microwelding of Pt-10 Pct Ir to 316 LVM Stainless Steel: Part II. Effect of Orientation on Joining Mechanism

Y.D. HUANG, A. PEQUEGNAT, G.S. ZOU, J.C. FENG, M.I. KHAN, and Y. ZHOU

With the increasing complexity of medical devices and with efforts to reduce manufacturing costs, challenges arise in joining dissimilar materials. In this study, the laser weldability of dissimilar joints between Pt-10 pct Ir and 316 low-carbon vacuum melted (LVM) stainless steel (SS) crossed wires was investigated by characterizing the weld geometry, joint strength, morphology of weld cross sections, and differences in joining behavior, depending on which material is subject to the incident laser beam. With the Pt-Ir alloy on top, a significant amount of porosity was observed on the surface of the welds as well as throughout the weld cross sections. This unique form of porosity is believed to be a result of preferential vaporization of 316 LVM SS alloying elements that become mixed with the molten Pt-10 pct Ir during welding. The joining mechanism documented in micrographs of cross-sectioned welds was found to transition from laser brazing to fusion welding. It is inferred that the orientation of the two dissimilar metals (*i.e.*, which material is subject to the incident laser beam) plays an important role in weld quality of crossed-wire laser welds.

DOI: 10.1007/s11661-011-1003-6

I. INTRODUCTION

SPECIAL requirements of materials used in implantable medical devices include biocompatibility, corrosion resistance, and the ability to produce joints of extremely high reliability.[1] Common materials that meet these requirements include 316 low-carbon vacuum melted (LVM) stainless steel (SS), titanium, niobium, NITINOL (Nickel Titanium Naval Ordnance Laboratory), platinum, platinum-iridium alloys, and nickel-cobalt alloys such as MP35N* and KOVAR.**[1] The excellent mechanical properties and electrical conductivity of Pt alloys and 316 LVM SS make them ideal for biomedical applications including electrical terminals, wires, coils, and electrodes.[2,3] With the increasing complexity of medical devices and a constant drive for lower costs, the challenge of joining dissimilar biocompatible materials arises.[4] For example, the electrical terminals in pacemakers are made of a Pt-Ir alloy, while the interconnecting wires are made from SS. To control material costs, it is necessary to join these dissimilar materials.

Resistance microwelding (RMW) and laser microwelding (LMW) are two of the most important joining processes applied to the small-scale fabrication of medical devices.[1,5–7] As acknowledged in recent publications, variations in resistivity and other material properties have hindered the application of RMW for dissimilar materials.[4,8–10] Therefore, study of dissimilar laser spot microwelding of the preceding materials is worth investigating.

Current literature on microwelding of crossed wires has focused on RMW processes applied to joining of bare and Au-plated Ni wires, 316 LVM SS, and 304 SUS SS.[6,7,11–13] However, only limited literature exists detailing the research on LMW of crossed wires. This is especially true for dissimilar material combinations. This study is a continuation of the work performed in Reference 14 with the objective of identifying the crossed-wire laser weldability of Pt-10 pct Ir to 316 LVM SS when the Pt-10 pct Ir wire is on top and subject to the laser energy. In the joining of dissimilar crossed wires, it is expected that the orientation or stacking order will have a significant effect on the joining behavior due to differences in material properties such as melting temperature, where the Pt-10 pct Ir alloy and the 316 LVM SS materials have a difference in melting

*MP35N is a trademark of SPS Technologies Inc., Jenkintown, PA.

**KOVAR is a trademark of Carpenter Technology Corporation, Wyomissing, PA.

Y.D. HUANG, PhD Student, with the State Key Laboratory of Advanced Welding and Joining, Harbin Institute of Technology, Harbin 150001, P.R. China, and is also a Visiting Scientist, with the Department of Mechanical and Mechatronics Engineering, University of Waterloo, ON N2L 3G1, Canada. Contact e-mail: huangydhm@gmail.com A. PEQUEGNAT, PhD Student, M.I. KHAN, Postdoctoral Student, and Y. ZHOU, Professor, are with the Department of Mechanical and Mechatronics Engineering, University of Waterloo. Contact e-mail: apequegn@uwaterloo.ca G.S. ZOU, Professor, is with the Department of Mechanical Engineering, Tsinghua University, Beijing 100084, P.R. China, and is also a Visiting Professor, with the Department of Mechanical and Mechatronics Engineering, University of Waterloo. J.C. FENG, Professor, is with the National Key Laboratory of Advanced Welding Production Technology, Harbin Institute of Technology.

Manuscript submitted September 2, 2010.
Article published online January 26, 2012

Table I. Chemical Composition of 316 LVM SS Wire (Weight Percent)

C	Mn	Si	Cr	Ni	Mo	P	S	Cu	N	Fe
0.024	1.84	0.75	17.47	14.73	2.76	0.017	0.001	0.04	0.024	bal

temperature of 200 K to 400 K. No literature on the effects of wire orientation on the LMW weldability of crossed-wire dissimilar welds currently exists. The current study will address the difference in joint morphology and joint breaking force (JBF) with increasing laser power. A comparison is made between the joints in this work, where the Pt-10 pct Ir wire was subject to the incident laser beam to joints made in a sister article,[14] where 316 LVM SS wire was subject to the incident laser beam. Furthermore, the porosity defect that arises when Pt-10 pct Ir wire was subject to the incident laser beam will be addressed providing significant scientific findings that are essential for dissimilar materials joining.

II. EXPERIMENTAL PROCEDURE

As was performed in Part I of this study,[14] fully annealed 0.38-mm-diameter Pt-10 pct Ir and spring-tempered 316 LVM SS wires were joined by laser spot microwelding. However, in this study, the Pt-10 pct Ir wire was subject to the incident laser beam rather than the 316 LVM SS wire. The chemical composition of the 316 LVM SS wire is shown in Table I. Before welding, the wires were ultrasonically cleaned in acetone for 10 minutes to remove any surface contaminants. Welding was conducted using a Miyachi Unitek LW-50A Nd:YAG laser welding system, capable of 50 J pulsed energy and 5 kW peak power. The pulse profile used consisted of a 0 ms up-slope, 30 ms weld time, followed by a 0 ms down-slope. The peak power was varied from 0.20 to 0.52 kW, and an argon shielding gas was used in this study.

Figure 1 shows the schematic of the welding fixture used to position the wires at 90 deg to one another. A small force was imposed by spring plates on the Pt wire located on the top to ensure intimate contact with the SS wire. A hole in the fixture located directly below the weld location prevented welding of the wires to the fixture. The hole had a depth (H) of 1 mm and a diameter (Φ) of 1 mm. Care was taken to ensure that each weld was centered at the intercept of the two wires. A positioning laser was used to accurately determine the center of each weld.

A schematic of the tensile testing method used to determine the JBF is shown in Figure 2. The joints were subject to a tensile-shear loading condition. The tensile tests were performed using an INSTRON† model 5548 microtensile tester with a crosshead speed of 4 mm/min. Three joints were tested for each set of welding conditions to obtain the average JBF.

†INSTRON is a trademark of Instron, Canton, MA.

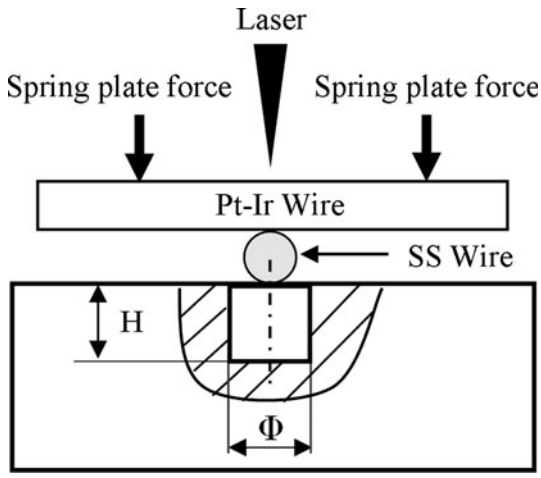

Fig. 1—Schematic of welding fixture, where H = 1 mm and Φ = 1 mm (not to scale).

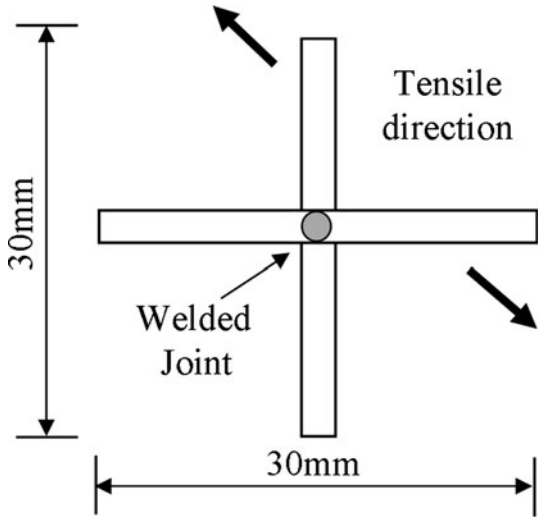

Fig. 2—Schematic of tensile test setup (not to scale). The large arrows indicate the direction of the applied tensile force. The joint is tested under a tensile-shear condition.

The surface appearance, fracture surfaces, and cross sections of the joints were examined using an energy dispersive X-ray spectrometer (EDX) equipped scanning electron microscope (SEM).

III. RESULTS

A. *Weld Geometry*

The top and bottom views of crossed-wire welds produced using peak welding powers of 0.28 to 0.52 kW are shown in Figure 3. At the lowest peak power of 0.28 kW, little change was observed on either the top or

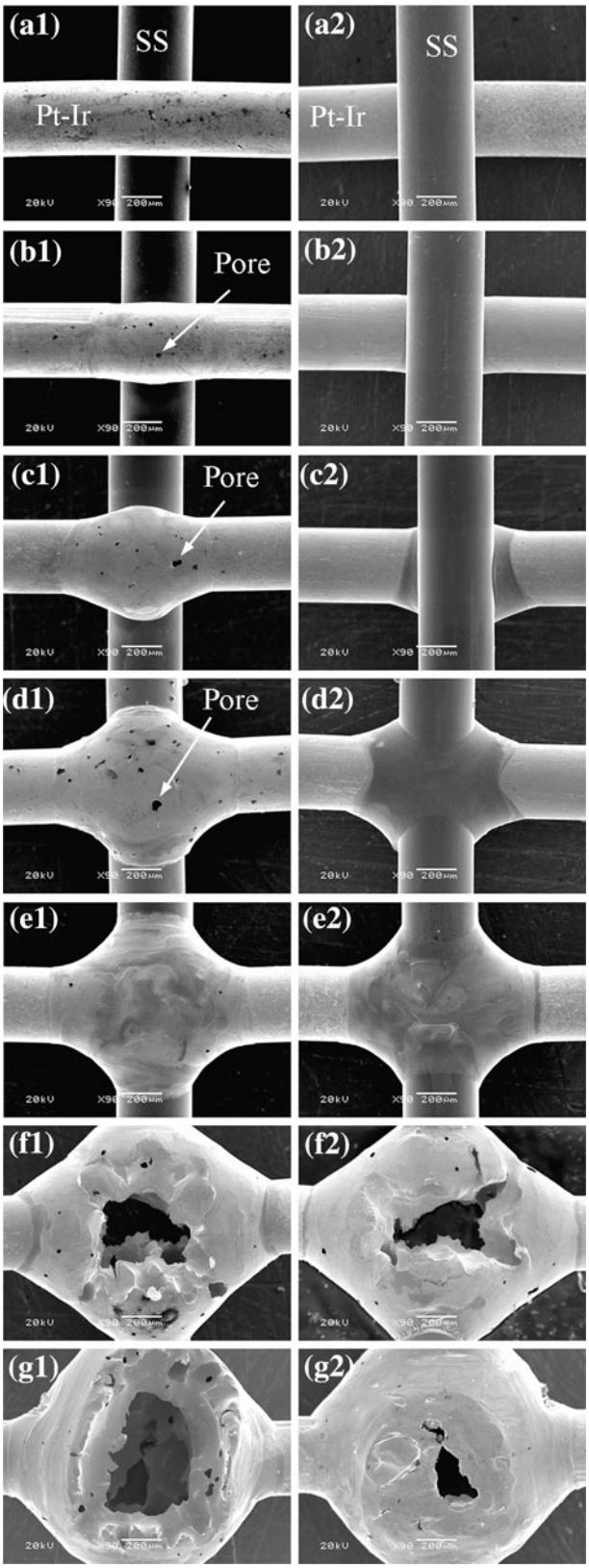

Fig. 3—(a1) through (g1) Top and (a2) through (g2) bottom surfaces of welded crossed-wire joints with laser peak powers of (*a*) 0.28 kW, (*b*) 0.32 kW, (*c*) 0.36 kW, (*d*) 0.40 kW, (*e*) 0.42 kW, (*f*) 0.46 kW, and (*g*) 0.52 kW.

bottom side of the joint (Figures 3(a1) and (a2)). For peak powers of 0.32 to 0.40 kW, surface pores were observed on the top side of the joint (*i.e.*, Pt-Ir wire side) that was subject to the incident laser beam (Figures 3(b1)\ through (d1)). The number and size of the pores increased with peak power. However, the surface porosity disappeared with a peak power of 0.42 kW. No porosity was found on the bottom side (*i.e.*, 316 LVM SS side) of the welds during this study. Increasing the peak power further caused the laser to drill through the weld, which caused burn-through type defects, as shown in Figures 3(f1) through (g1) and (f2) through (g2) for peak powers of 0.46 and 0.52 kW, respectively.

With increasing peak power, the weld geometry transitioned from insufficient melting to a smooth acceptable geometry and then finally to an overwelded condition. From a surface quality and weld geometry perspective, welds produced with a peak power of 0.42 kW were considered to be acceptable due to the smooth surface and complete set-down of the Pt-Ir wire into the SS wire (Figures 3(e1) and (e2)). Mixing of the two molten alloys was observed with peak powers above 0.36 kW, as shown in Figures 3(c) through (g), where obvious contrast differences were visible on the surfaces of the welds.

B. *JBF and Fracture Mode*

The effect of peak power on the JBF is shown in Figure 4. At low peak powers from 0.26 to 0.32 kW, the joint strength increased rapidly with increasing power. At a peak power of 0.32 kW, the JBF reached 37.4 N, which is 87 pct of the 43 N tensile strength of the Pt-10 pct Ir wire. Through the intermediate power range between 0.32 and 0.42 kW, the JBF remained constant when considering the standard deviation of the data. The JBF decreased for joints made with a peak power above 0.42 kW due to overwelding.

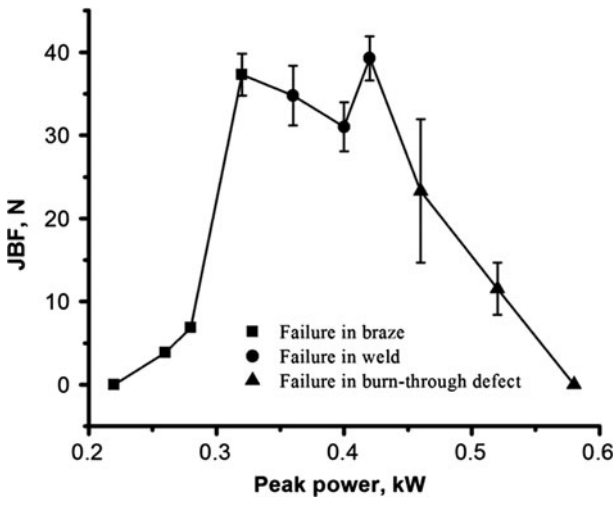

Fig. 4—JBF *vs* peak power (failure modes indicated).

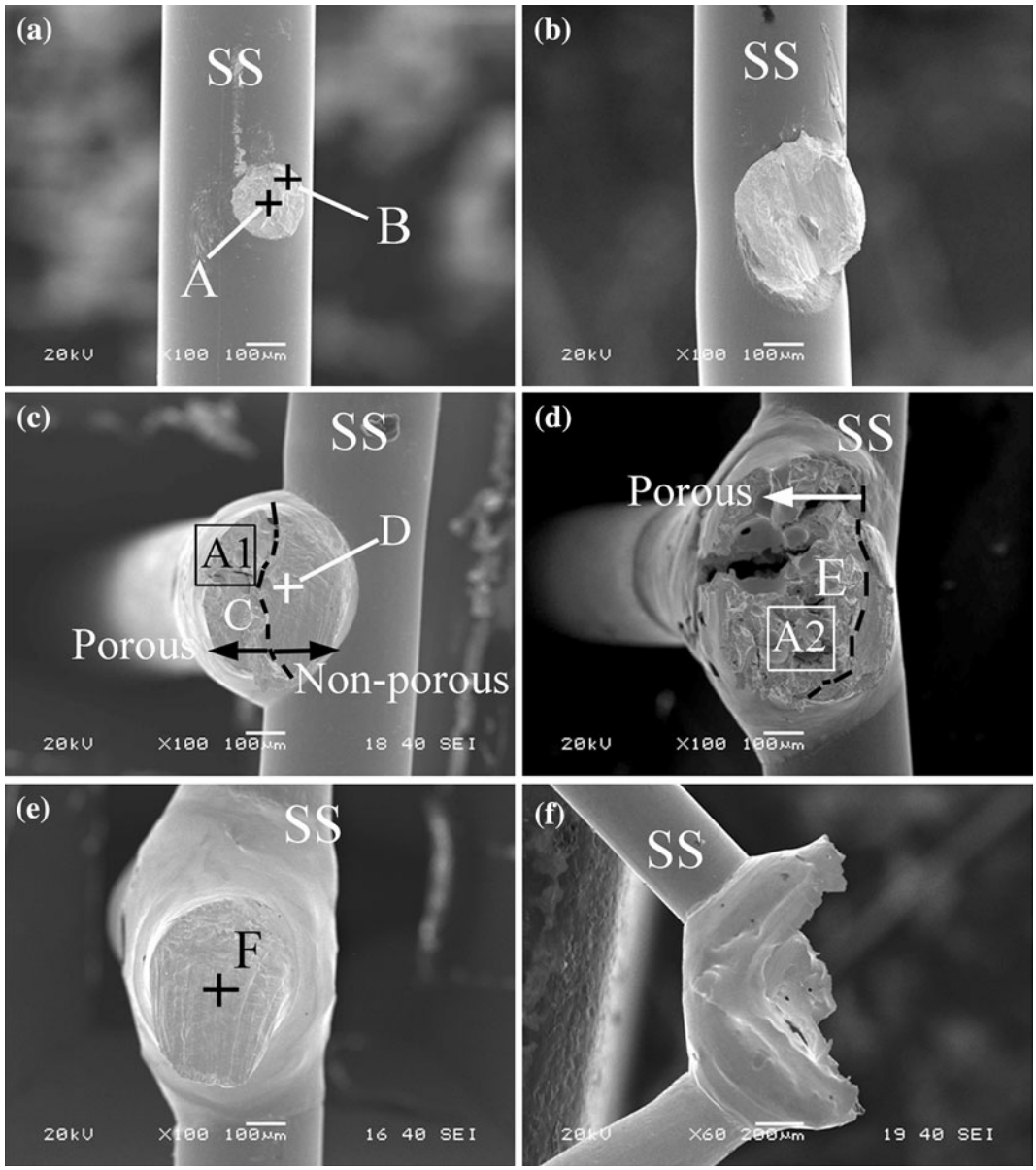

Fig. 5—SEM images of tensile specimen fracture surfaces from joints welded with various peak powers of (*a*) 0.28 kW, (*b*) 0.32 kW, (*c*) 0.36 kW, (*d*) 0.40 kW, (*e*) 0.42 kW, and (*f*) 0.46 kW.

After measurement of the JBF, the fracture surfaces of the specimens were examined using SEM and EDX. Figure 5 shows SEM images of the fracture surfaces. The results from an EDX analysis of points A through F in Figure 5 are given in Table II. The joints welded at peak powers of 0.28 and 0.32 kW showed increasing joint area with increasing peak power, as shown in Figures 5(a) and (b). This increase in joint area coincided with the increase in JBF. Based on the results from the EDX analysis, points A and B showed that the fracture occurred through a mixed region of the joint, where Pt, Ir, Fe, Ni, and Cr elements were present. The fracture surface of the 0.36 kW sample, shown in Figure 5(c), contained a porous region (point C) and a nonporous region (point D). The fracture surface of the 0.40 kW sample, shown in Figure 5(d), showed an increase in the size of the porous region compared to the 0.36 kW sample. From the EDX analysis of the region containing pores, the weld metal was found to be a mix of Pt, Ir, Fe, Ni, and Cr (points C and E). The nonporous region, however, contained mostly Pt and Ir, as measured near the boundary between the porous and nonporous regions at point D in Figure 5(c). High-magnification SEM images shown in Figure 6 of region A1 from Figure 5(c) and region A2 from Figure 5(d) showed an increase in the size of the pores with increasing peak power. Fractography of the joint produced with a peak power of 0.42 kW showed fracture occurring at the outer edge of the welded joint in the Pt-Ir wire, as shown in Figure 5(e). This failure mode produced the maximum JBF of 39.3 N, which coincides with the absence of surface pores. The reason

Table II. EDX Analysis Results from Fracture Surfaces Shown in Fig. 5 (Atomic Percent)

Position	Pt	Ir	Fe	Cr	Ni	Other Elements
A	84.17	7.93	—	1.07	5.19	1.64
B	78.56	4.77	8.91	2.28	—	5.49
C	60.55	5.91	20.26	5.74	3.61	3.93
D	87.85	7.56	4.60	—	—	—
E	47.58	5.17	27.86	8.36	6.47	4.56
F	86.31	9.75	3.94	—	—	—

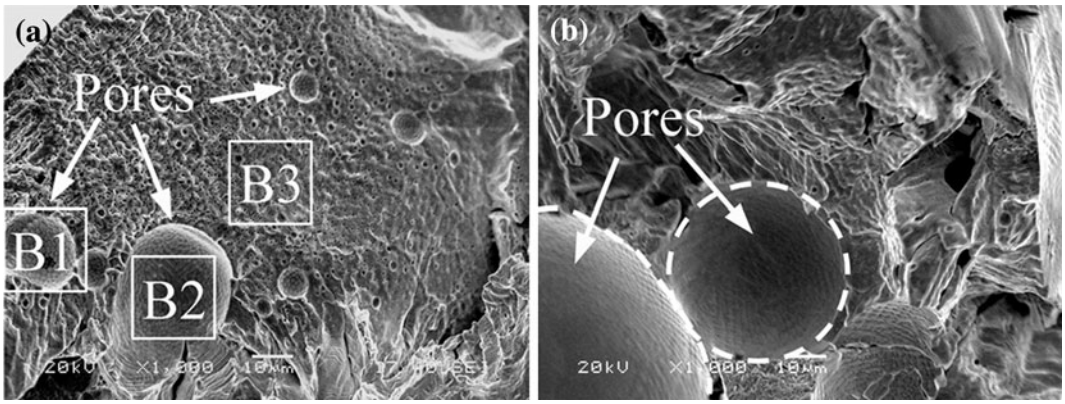

Fig. 6—High-magnification SEM images of porosity in the fracture surface of welds produced with peak powers of (*a*) 0.36 kW and (*b*) 0.40 kW from Fig. 5 regions A1 and A2, respectively.

for lack of surface porosity at a peak power of 0.42 kW is unknown. Joints produced with a peak power above 0.42 kW fractured along the burn-through defects produced by overwelding, as shown in Figure 5(f). These burn-through defects caused the JBF to decrease.

C. *Joint Cross Sections*

Scanning electron micrographs of welds cross sectioned along the Pt-Ir wire axis are shown in Figure 7. At the low peak power of 0.28 kW, as shown in Figures 7(a) and 8(a), melting began at the interface, and the downward force on the Pt-Ir wire from the welding fixture caused the molten metal to be expelled from the interface. Based on the EDX results in Table III, the melted material at the interface and the expelled material were mixtures of Pt, Ir, Fe, Ni, and Cr (points C2 and C3). With the increase of the peak power to 0.32 kW, more set-down of the Pt-Ir wire occurred and a smooth fillet was formed between the Pt-Ir and SS wires caused by wetting of the joint with the molten metal, as shown in Figure 7(b). As the power was increased further to 0.36 and 0.40 kW, porosity began to occur at the top of the weld, as shown in Figures 7(c) and (d). The size and number of pores increased from 0.36 to 0.40 kW. At a peak power of 0.42 kW, as shown in Figure 7(e), only a few large pores remained and surface porosity was not found. Undercutting was also observed with peak powers above 0.42 kW.

A difference in contrast was observed at the top of the joint in welds made with a peak power above 0.36 kW, as shown in Figures 7(c) and (d). An EDX analysis of the 0.40 kW weld from the top surface of the joint through to the bottom of the joint, as shown in Figure 8(b), showed that there were three distinct regions with different compositions (Table IV). These regions included a porous darker region on the top of the Pt-Ir wire composed of a mixed zone (MZ) of Pt, Ir, Fe, Ni, and Cr (points D1 and D2), a light region composed of Pt and Ir (point D3), and a dark region at the bottom of the weld composed mainly of the SS alloying elements (points D4 and D5).

IV. DISCUSSION

A. *Joint Formation*

An illustration of the joint formation is shown in Figure 9 to aid in this discussion. The joining mechanism transitioned from a laser-brazed joint to a fusion weld as the peak power was increased. For joints made with laser peak powers between 0.28 and 0.40 kW, a laser braze type joint was formed between the Pt-Ir and SS wires, as shown in Figure 10. The nature of this braze will be discussed in the next paragraph. The volume of braze available to wet the Pt-Ir wire increased with laser power. With a peak power above 0.32 kW, enough braze was available to wet the entire joint, as shown in Figures 11(a) and (b). Once the braze wetted the entire joint, a MZ was formed, as illustrated in Figures 9(b) and (c). The depth of the MZ increased with increasing power until full penetration through the Pt-Ir wire was achieved and a fusion weld was formed, as illustrated in Figures 9(b) through (d). Fusion welding occurred with peak powers above 0.4 kW, where complete melting of

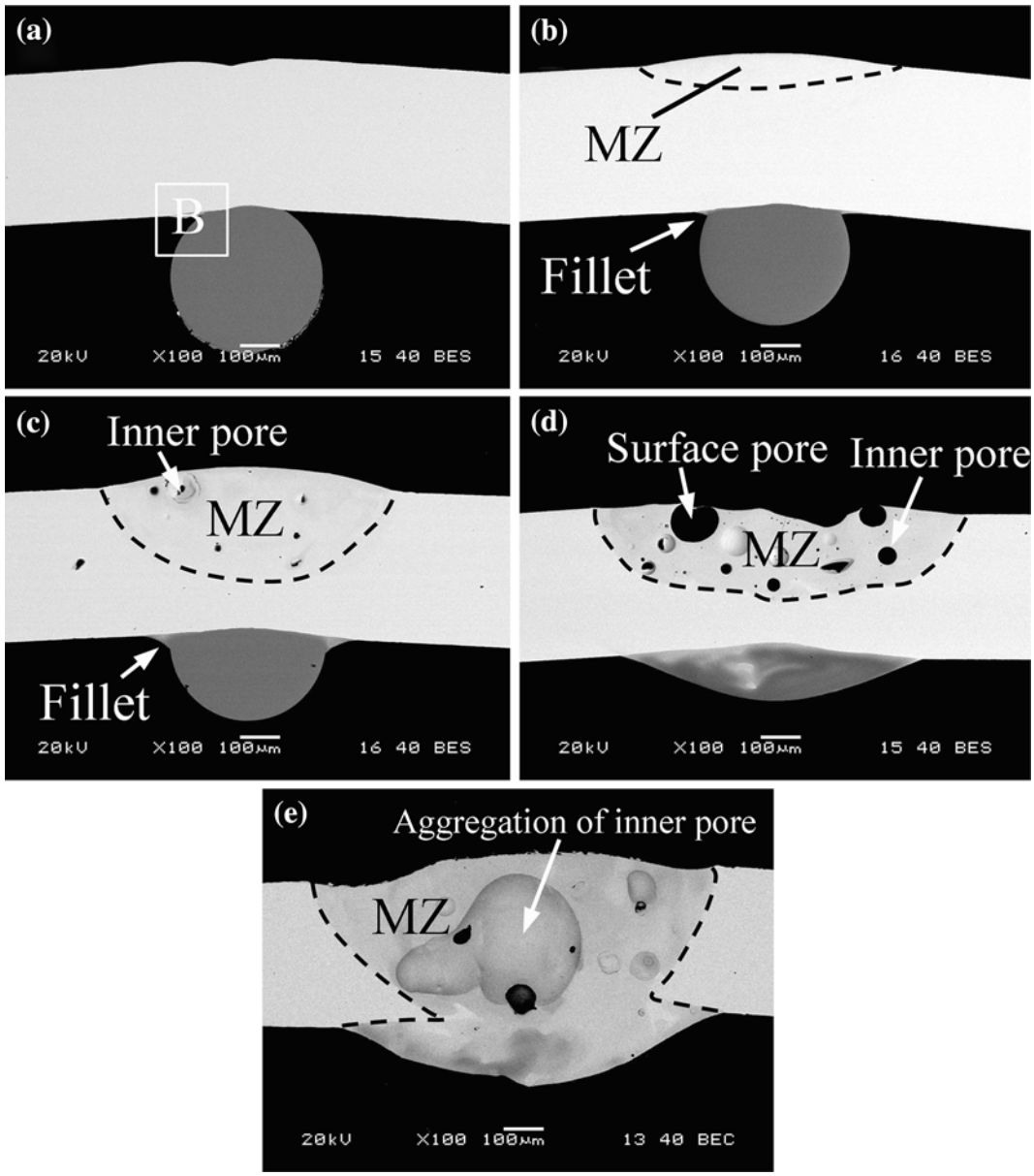

Fig. 7—SEM images of joint cross sections along the Pt-Ir wire axis. Weld produced with (*a*) a peak power of 0.28 kW, (*b*) a peak power of 0.32 kW, (*c*) a peak power of 0.36 kW, (*d*) a peak power of 0.40 kW, and (*e*) a peak power of 0.42 kW. The dashed lines highlight the MZ, where elements from each of the wire materials are found.

Table III. EDX Analysis Results of Regions C1, C2, C3, and C4 from Fig. 8 (Atomic Percent)

Position	Pt	Ir	Fe	Cr	Ni	Other Elements
C1	74.47	9.52	1.63	—	4.30	10.09
C2	25.01	4.05	46.66	13.33	9.89	1.06
C3	11.96	2.61	51.49	14.19	15.16	4.59
C4	0.35	—	60.13	20.82	13.03	4.68

both wires was achieved and complete mixing occurred in the molten weld pool.

The temperatures in different regions of the joint could be deduced by observing the unique sample cross sections and considering the three distinct regions observed in the 0.40 kW joint shown in Figures 7(d) and 8(b). The temperature in the MZ must be higher than 2053 K to 2078 K (1780 °C to 1805 °C), the melting range of the Pt-Ir wire,[15] in order for mixing of the Pt-Ir and the braze metal to occur. The lighter region in between the MZ and the braze at the bottom of the joint was noted to be unmelted Pt-Ir wire.

Therefore, the temperature in this region must have been below 2053 K (1780 °C). The temperature of the braze was assumed to be above 1643 K to 1673 K (1370 °C to 1400 °C), the melting range of SS, but below 2053 K (1780 °C). A low melting point mixture of the Pt-Ir and SS alloying elements, however, could also be possible, leading to braze liquid being formed below the melting point of both the Pt-Ir and SS wire materials. Complexities due to the number of alloying elements in the SS wire have made identifying a single low melting point composition, as was done in Reference 11, difficult.

There are several differences in the joint formation when the Pt-Ir wire was subject to the incident beam compared to what was found in Part I[14] of this study when the SS wire was subject to the incident beam. When the Pt-Ir wire was on top initially, the SS wire below melted due to conduction of heat through the unmolten Pt-Ir wire rather than from the laser energy itself. This leads to a braze type joint at low laser peak powers, where the molten SS material wets the Pt-Ir wire from below. This was caused by the substantially lower melting range of the 316 LVM SS wire material. With increasing power, the top of the Pt-Ir wire on which the laser was focused becomes molten and the elements from the SS braze mix with the molten Pt-Ir and create an MZ. As the power was increased further, the depth of the MZ increased until full penetration occurred. Significant porosity was realized once the MZ was established. On the contrary, when the SS wire was subject to the incident laser beam, it was melted directly by the laser energy and wet the Pt-Ir wire below, creating a brazed joint.[14] In this case, only a small portion of the Pt-Ir wire became molten until the power was increased above 0.39 kW, where full penetration was achieved. The amount of Pt and Ir mixed in the molten SS material was minimal, and porosity was not observed until full penetration occurred. The maximum JBF produced was found to be similar regardless of wire orientation; however, severe porosity defects reduce the joint quality of joints produced, where the Pt-Ir wire was subject to the incident laser beam.

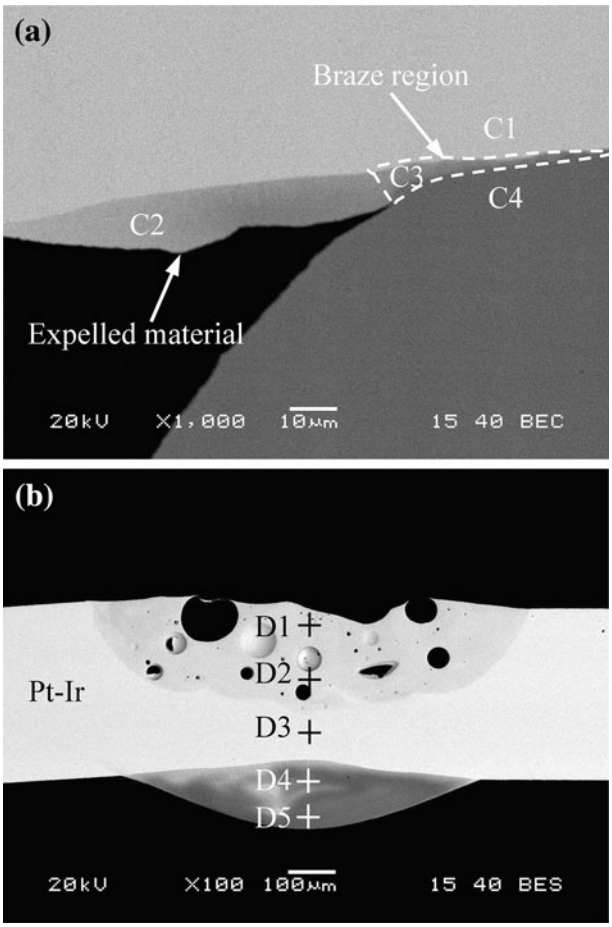

Fig. 8—High-magnification SEM image of (*a*) joint produced with a peak power of 0.28 kW from region B of Fig. 7 and (*b*) EDX analysis points across 0.40 kW weld cross sectioned along the Pt-Ir wire axis.

B. *Porosity Defect*

A large amount of porosity was observed in the MZ of welds produced at the peak powers of 0.36 and 0.40 kW, as shown in Figures 7(c) and (d). The amount of pores and their size increased with increasing peak power, where at 0.42 kW, one large pore was found at the center of the weld shown in Figure 7(e).

It is well known that laser welding can induce porosity in the weld metal due to vaporization caused by high peak temperatures and the inherent high cooling rates, which allow insufficient time for trapped gasses to escape during solidification.[16–19] More specifically, porosity was attributed to changes in solubility of hydrogen in Al and Mg alloys during solidification,[16,18] volatilization of high vapor pressure alloying elements,[18,20] and instability during keyhole welding, leading to entrapped shielding gas, air, or volatile alloying elements.[19,21] No porosity was observed when joining Pt-10 pct Ir wires to themselves in unpublished work or when joining 316 LVM SS wires, as was performed by Khan *et al.*[4] However, in this study, it was found that porosity occurs when joining the two dissimilar materials together in the MZ of the joint. As the molten braze mixed with the molten Pt-Ir weld

Table IV. EDX Analysis Results of Regions D1, D2, D3, D4, and D5 from Fig. 8 (Atomic Percent)

Position	Pt	Ir	Fe	Cr	Ni	Other Elements
D1	47.89	7.34	28.72	6.67	7.57	1.81
D2	54.82	7.30	23.72	7.43	3.93	2.81
D3	85.50	12.78	—	—	—	1.72
D4	14.42	1.68	49.87	16.49	12.43	5.11
D5	0.10	0.01	62.71	18.03	13.22	5.93

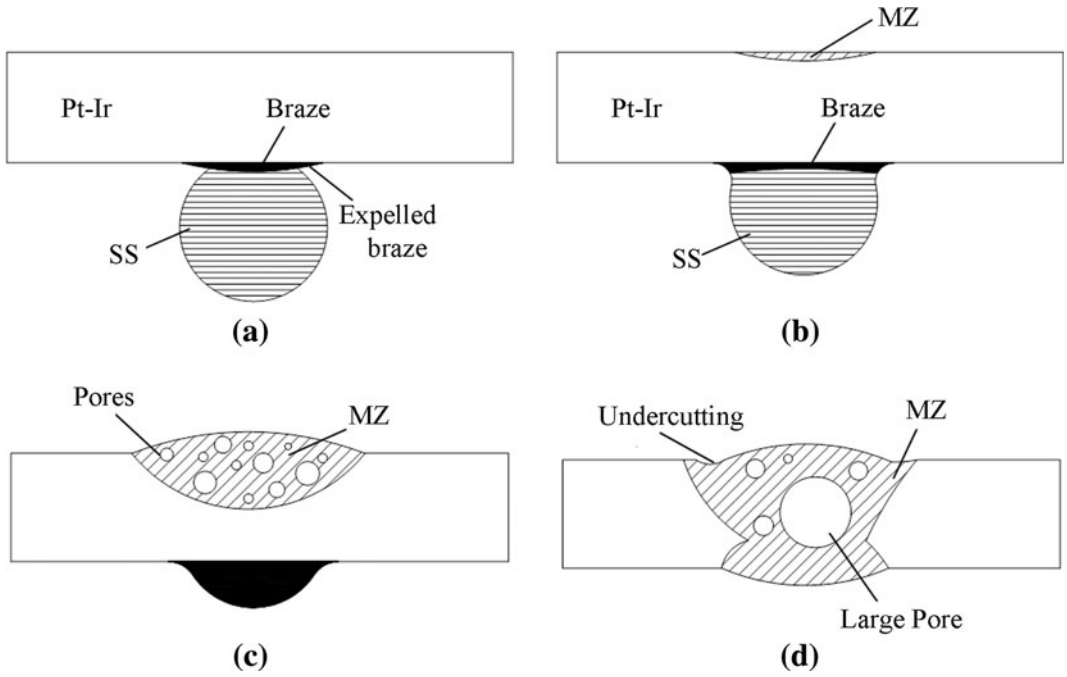

Fig. 9—Illustration of joint formation with increasing peak power from (*a*) to (*d*) (not to scale). (a) Incomplete wetting, (b) complete wetting, (c) complete wetting with porosity, and (d) fusion weld.

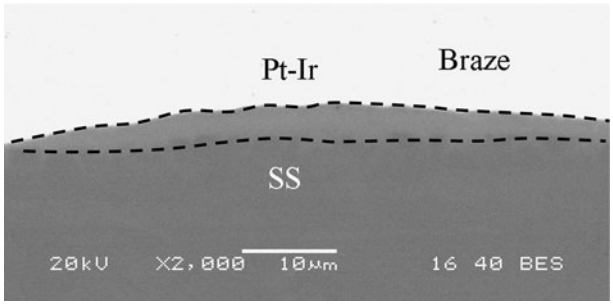

Fig. 10—High-magnification image of brazed joint produced with a peak power of 0.28 kW.

pool to create the MZ, it is quite plausible that the Fe, Ni, and Cr elements are preferentially vaporized due to their relatively higher vapor pressures, promoting porosity. The volatilization of SS alloying elements reported by He *et al.*[22] and the preferential volatilization of Mg and Zn in aluminum alloys reported by Haboudou *et al.*[18] are examples of volatilization of high vapor pressure alloying elements. Matsunawa *et al.*[19] showed that the volatilization of alloying elements contributes to porosity formation during laser welding by directly observing the keyhole and vapor plume by means of X-ray transmission imaging.

Since the primary driving force for vaporization is the total pressure gradient at the elevated temperatures experienced in the weld pool, the likelihood for volatilization of each element in the MZ can be obtained using thermodynamic principles.[22] The preferential vaporization of these elements can be predicted by calculating the equilibrium vapor pressures $\left(p_{\mathrm{i}}^{o}\right)$ over their pure liquid.[22,23] The equilibrium vapor pressures of the elements in the MZ are plotted in Figure 12(a) with respect to temperature.[23] The vapor pressures of Fe, Ni, and Cr increase much faster with temperature compared to those of Pt and Ir. This indicates that Fe, Ni, and Cr will preferentially vaporize in their pure liquid. However, when considering the vapor pressure of each element in the MZ and the vaporization flux, the mole fraction of each element in the MZ must be considered.[22] The vapor pressure of each element in the MZ (p_i) can be found by using the equation[22]

$$p_{\mathrm{i}} = X_{\mathrm{i}} p_{\mathrm{i}}^{o} \qquad [1]$$

where X_{i} is the mole fraction of element "i" in the MZ and p_{i}^{o} is the equilibrium vapor pressure of element i over the pure liquid. The vapor pressure of each element in the MZ is plotted in Figure 12(b) at 3000 K (2727 °C) using the MZ elemental composition at point D1 given in Table IV. Again, Fe, Ni, and Cr have substantially larger vapor pressures compared to Pt and Ir. After considering the mole fraction of each element in the MZ, Fe will be the most likely to vaporize and will have the largest vaporization flux, followed by Ni and Cr. These results correlate well with the findings of He *et al.*[22] when studying alloying element vaporization during pulsed Nd:YAG laser welding of 304 SS. Also, in Table V, the results from the EDX analysis of pores (Figure 6(a), regions B1 and B2) and the MZ (Figure 6(a), region B3) of the fracture surface, the Fe content in the pores was found to be at least 30 pct higher than that of regions in between the pores. The inner walls of the previously entrapped pores contained higher levels of Fe due to the solidification of the metal vapor as the weld pool solidified. This further suggests that the vaporization of alloying elements plays an important role in the porosity

observed in the MZ. A similar analysis was carried out by Haboudou *et al.*[18] and Matsunawa *et al.*,[19] investigating porosity in Al alloys.

Due to the complexity of the dissimilar crossed-wire joint studied in this work, it was difficult to determine the laser welding mode. Due to the amount of porosity, it is logical to believe that there was instability in the weld pool, suggesting a transition mode in between the conduction welding mode keyhole welding mode. This transition mode was attributed to causing the most severe porosity in several different studies.[19,21] At 0.42 kW, the single large pore at the center of the cross section is characteristic of the collapse of the keyhole, further suggesting keyhole welding during the high peak power full penetration fusion welds.[21] As a result, the pores most likely contain a mixture of entrapped Ar shielding gas, air, and condensed metal vapor. Porosity occurring only when the Pt-Ir wire was subject to the incident beam can be explained by the differences in composition of the MZ and the thermal gradient in the joint depending on which wire material was on top. When the Pt-Ir wire was on top, relatively large percentages of the SS alloying elements were mixed in the MZ, leading to higher partial pressures complying with Eq. [1]. This was not the case when the SS wire material was subject to the incident laser beam.[14] When

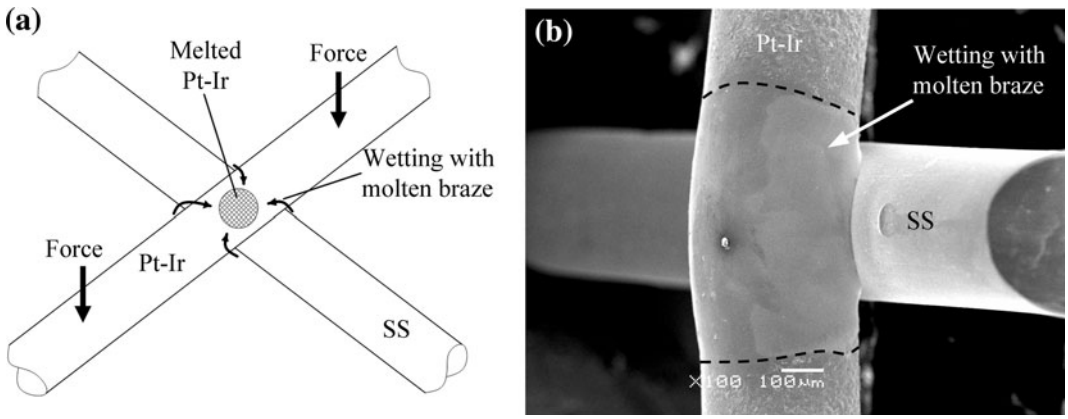

Fig. 11—(*a*) Molten braze from the bottom of the joint wets the entire surface of the Pt-Ir wire. (*b*) SEM image of the wetting of the Pt-Ir wire with molten SS in a joint formed with 0.32 kW peak power. The braze mixes with the molten Pt-Ir at the top of the joint to create the MZ observed in the crossed-sectioned samples.

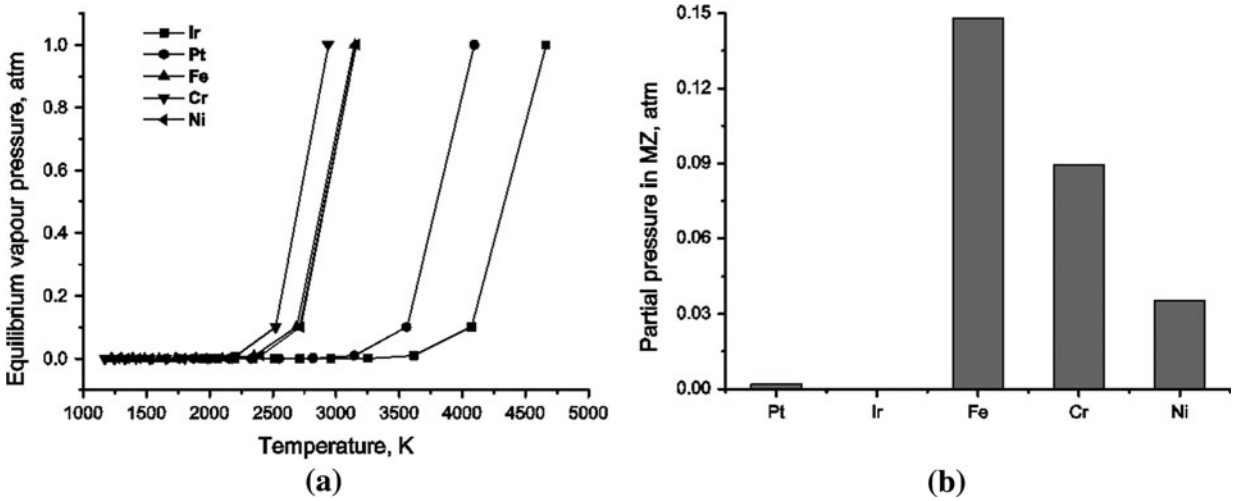

Fig. 12—(*a*) Equilibrium vapor pressure of alloying elements as a function of temperature. (*b*) Partial pressure of alloying elements in the MZ at a temperature of 3000 K (2727 °C).

Table V. EDX Analysis Results of Regions B1, B2, and B3 from Fig. 6 (Atomic Percent)

Position	Pt	Ir	Fe	Cr	Ni	Other Elements
B1	46.64	—	28.30	—	14.43	10.62
B2	45.55	6.56	45.45	—	—	2.44
B3	62.63	8.57	14.27	1.84	5.97	6.72

considering the thermal gradient, the MZ does not occur predominately at the weld surface, the highest temperature region, where vaporization is most likely to occur when the SS wire is subject to the incident beam.[14] As a result, the temperature in the MZ may not reach a degree high enough to cause vaporization. Furthermore, the Pt-Ir wire has a thermal diffusivity of 24 times that of SS,[10] leading to higher freezing rates and less time for entrapped gasses to escape *via* buoyancy forces.

C. *Importance of Wire Orientation*

The joint formation for the dissimilar crossed-wire welds is greatly influenced by the temperature gradient in the joint during welding, as well as by the properties of the wire materials being joined. In this study, the Pt-10 pct Ir wire was exposed to the incident beam and a porous MZ resulted from the mixing of the *in-situ* formed braze alloy with molten Pt-Ir, even at moderate peak powers. Due to the difference in melting temperature and the temperature gradient in the joint during welding, only the top of the Pt-Ir wire was melted while the SS wire below became fully molten, leading to mixing of the two materials and undesirable porosity defects. In contrast, in Part I of this study,[14] where the SS wire was exposed to the incident beam, a brazed type joint was produced in which the SS material acted as a braze at low peak powers with little melting of the Pt-Ir wire. Mixing of molten SS and Pt-Ir was minimized, which reduced or at the lower peak powers eliminated porosity. Similar JBF values were achieved with either wire orientation; however, 33 pct lower peak powers were used in Part I of this study[14] and porosity was avoided.

V. CONCLUSIONS

The laser weldability of Pt-10 pct Ir and 316 LVM SS crossed wires, with the Pt-10 pct Ir wire exposed to the incident laser beam, were investigated by characterizing the weld geometry, measuring the JBF, and studying the morphology of weld cross sections. The major conclusions are summarized as follows.

1. The joining mechanism of the crossed wires transitioned from a laser braze to a fusion weld with increasing peak power. Due to the 26 pct higher melting temperature of the Pt-10 pct Ir wire compared to the 316 LVM SS wire, the *in-situ* formed braze alloy was predominantly SS material at low peak power. A peak power above 0.42 kW was required for complete fusion welding, where both the Pt-Ir and SS wires became molten and mixing occurred across the entire joint.
2. The optimum joint geometry and a JBF value of 91 pct of the tensile strength of the Pt-10 pct Ir wire was achieved with a peak power of 0.42 kW when no surface pores were present. Large pores, however, were found in the cross sections of the welds.
3. A unique form of porosity in the weld was believed to be caused by the preferential vaporization of the Fe, Ni, and Cr in the MZ. The MZ results from the unique joint formation caused by the dissimilar wire properties and joint orientation.
4. The material orientation must be considered along with the temperature gradient and material properties in the laser welding of dissimilar crossed wires. Acceptable LMW welds between dissimilar Pt-10 pct Ir and 316 LVM SS wires were only possible when the SS wire was subject to the incident laser beam.

ACKNOWLEDGMENTS

This work was funded by the Program of Canada Research Chairs (CRC) in Microjoining (www.crc.gc.ca). A special thanks goes out to B. Tam for helping with the preparation of the welded samples. The help of Professor W.H.S. Lawson in reviewing this manuscript is greatly appreciated.

REFERENCES

1. *Microjoining and Nanojoining*, Y. Zhou, ed., Woodhead Publishing Ltd., Cambridge, United Kingdom, 2008.
2. J. Xie and S. Safarevich: *Proc. Materials and Process for Medical Devices Conf. (MPMD)*, Anaheim, CA, Sept. 2003, pp. 25–30.
3. N.J. Noolu, H.W. Kerr, Y. Zhou, and J. Xie: *Mater. Sci. Eng. A*, 2005, vol. 397, pp. 8–15.
4. I. Khan and Y. Zhou: *Proc. Materials and Processes for Medical Devices Conf. (MPMD)*, Palm Springs, CA, Sept. 2007, pp. 38–41.
5. D.R. Haynes, T.N. Crotti, and M.R. Haywood: *J. Biomed. Mater.*, 2000, vol. 49 (2), pp. 167–75.
6. S. Fukumoto and Y. Zhou: *Metall. Mater. Trans. A*, 2004, vol. 35A, pp. 3165–76.
7. S. Fukumoto, Z. Chen, and Y. Zhou: *Metall. Mater. Trans. A*, 2005, vol. 36A, pp. 2717–24.
8. Z. Chen: *J. Mater. Sci.*, 2007, vol. 42, pp. 5756–65.
9. K.J. Ely and Y. Zhou: *Sci. Technol. Weld. Join.*, 2001, vol. 6 (2), pp. 63–72.
10. Y.D. Huang, A. Pequegnat, J.C. Feng, M.I. Khan, and Y. Zhou: *Sci. Technol. Weld. Join.*, 2011, vol. 16 (7), pp. 648–56.
11. W. Tan, Y. Zhou, and H.W. Kerr: *Metall. Mater. Trans. A*, 2002, vol. 33A, pp. 2667–76.
12. M.I. Khan, J.M. Kim, M.L. Kuntz, and Y. Zhou: *Metall. Mater. Trans. A*, 2009, vol. 40A, pp. 910–19.
13. S. Fukumoto, T. Matsuo, H. Tsubakino, and A. Yamamoto: *Mater. Trans.*, 2007, vol. 48 (4), pp. 813–20.
14. G.S. Zou, Y.D. Huang, A. Pequegnat, X.G. Li, M.I. Khan, X.B. Hu, and Y. Zhou: *Metall. Mater. Trans. A*. DOI:10.1007/s11661-011-0763-3.
15. *Binary Alloy Phase Diagrams*, T.B. Massalski, ed., ASM INTERNATIONAL, Materials Park, OH, 1990, vol. 3, p. 2344.
16. L. Yu, K. Nakata, and J. Liao: *Sci. Technol. Weld. Join.*, 2009, vol. 14 (6), pp. 554–58.
17. S. Beretta and B. Previtali: *Sci. Technol. Weld. Join.*, 2009, vol. 14 (2), pp. 106–16.
18. A. Haboudou, P. Peyre, A.B. Vannes, and G. Peix: *Mater. Sci. Eng. A*, 2003, vol. A363, pp. 40–48.
19. A. Matsunawa, M. Mizutani, S. Katayama, and N. Seto: *Weld. Int.*, 2002, vol. 17 (6), pp. 431–37.
20. *AWS Welding Handbook*, 9th ed., vol. 3, *Welding Processes Part 2*, American Welding Society, Miami, FL, 2007.
21. M. Pastor, H. Zhao, R.P. Martukanitz, and T. Debroy: *Weld. J.*, 1999, vol. 78 (6), pp. 207s–216s.
22. X. He, T. DebRoy, and P.W. Fuerschbach: *J. Phys. D: Appl. Phys.*, 2003, vol. 36, pp. 3079–88.
23. R. Hultgren, R.L. Orr, P.D. Anderson, and K.K. Kelley: *Selected Values of Thermodynamic Properties of Metals and Alloys*, John Wiley & Sons, Inc., New York, NY, 1963.